Late Cenozoic glacial erosion and relief change in Fjord Steffen and Cordón Los Ñadis of the Patagonian Andes from apatite (U-Th)/He thermochronometry

Ryan A. Laemel
Advisor: Dr. Mark T. Brandon
Second Reader: Dr. David A. Evans

Wednesday, April 30, 2014

A Senior Thesis presented to the faculty of the Department of Geology and Geophysics, Yale University, in partial fulfillment of the Bachelor's Degree.

Abstract

Understanding late Cenozoic topographic evolution of the Patagonian Andes requires chronologic data on the growth and denudation of the mountain belt. Because thermochronologic data provide proxies for uplift and denudation, they can be used to reconstruct the tectonomorphic history of a region. Recent thermochronologic studies of the Patagonian Andes have evaluated the role of glaciation in landscape evolution (Mercer and Sutter, 1982; Thomson et al., 2001; Thomson et al., 2010). Several studies have proposed that buzzing glaciers limit the height of mountains (Porter and Skinner, 1987; Broecker and Denton, 1989; Thomson et al., 2010). Ma et al. (in review) used glacial modeling to show that not only were large ice caps the dominant mode of glaciation in the Patagonian Andes since the onset of glaciation at ~6 Ma but also that these glaciations produced large increases in regional relief. However, few studies of the Patagonian Andes have investigated how late Cenozoic glaciations gouged the landscape and affected local topographic relief development. We present 15 new apatite-helium cooling ages from samples collected in two parts, Fjord Steffen and Cordón Los Ñadis, of the Patagonian Andes to determine what, if any, changes in relief have occurred since closure at each location. We interpret age-elevation profiles according to the methods described in Braun (2002) to estimate erosion rates and relief change for the two sampling locations. Assuming no change in relief, i.e. $\beta = 1$, we report an erosion rate of 2.2 km/m.y. and, using a regional erosion rate of 0.2-0.4 km/m.y. from Herman and Brandon (in review), we find $\beta < 1$ for the Fjord Steffen area, indicating relief has decreased since the onset of glaciation. Assuming $\beta = 1$, we report an erosion rate of 0.45 km/m.y. for Cordón Los Ñadis. Because the erosion rate we find for Cordón Los Ñadis is close to the regional erosion rate of 0.2-0.4 km/m.y. from Herman and Brandon (in review), we resolve that there has been no change in relief in the Cordón Los Ñadis region since the initiation of glaciation. We conclude that the pre-glacial topography of the Patagonian Andes had either the same or higher relief than the modern topography and that valley depth has not increased since the onset of glaciation.

1. Introduction

The modern Patagonian Andes [Fig. 1] has experienced the competing forces of mountain building and denudation since ~25 Ma (Pardo-Casas and Molnar, 1987; Somoza, 1998; Thomson et al., 2001). Fluvial incision and hillslope mass transport were the dominant erosional processes until large-scale glaciation occurred as early as 7 Ma and continued as late as 20-15 kA, contemporaneous with the Last Glacial Maximum (LGM) (Mercer and Sutter, 1982; Thomson et al., 2001; Kaplan et al., 2005; Thomson et al., 2010; Ma et al., in review). Findings from thermochronometric studies of the Patagonian Andes have provided conflicting views of how glaciers erode landscapes. On one hand, several thermochronometric studies have supported (Thomson, 2002; Egholm, 2009) and elucidated (Thomson et al., 2010) the hypothesis put forth by Porter and Skinner (1987), and popularized by Broecker and Denton (1989), that buzzing glaciers have limited the height and growth of the Andes. On the other hand, Ma et al. (in review) found that large ice caps were the main form of glaciation and responsible for large relief development in the Patagonian Andes since ~6 Ma. The fact that different thermochronologic datasets and methods have produced conflicting opinions on how glaciers erode the landscape and enhance relief in the Patagonian Andes suggests that a better understanding of the dynamic between glacial erosion and the formation of relief is needed. Low temperature thermochronometry can be used to study how surface processes like glacial erosion produce changes in relief (Braun, 2002; Braun, 2006).

Tectonically active orogens like the Patagonian Andes are subject to exhumation, a process by which rock is brought up from deep in Earth's lithosphere and cooled (Braun, 2006). Because temperature increases with depth in the crust and some minerals contain elements that undergo nuclear decay reactions for which the products can be measured, thermal information can be converted to structural information and thus thermochronometric data can be used to estimate the time at which a mineral passed through a specific temperature in the subsurface; this temperature is known as the closure temperature of the thermochronometer (Dodson, 1973; Braun, 2002; Braun, 2006). Low temperature thermochronometric systems, e.g. the apatite (U-Th)/He system, having shallow isotherms that mimic the shape of the topography at the surface, are often used to quantify relief change caused by glacial erosion (Braun, 2006; Valla et al., 2011; Valla et al., 2012; Ma et al., in review).

Figure 1. Screenshot of the Andes from NASA's World Wind, a compilation of satellite images that constructs a virtual globe (from U.S. Government, NASA, World Wind).

Due to its remote location and lack of infrastructure, landscape evolution of the Patagonian Andes has been poorly studied (Thomson et al., 2001). The aim of this study is to use new apatite-helium cooling ages collected from the Patagonian Andes to resolve what, if any, changes in relief have occurred since closure. If large ice caps were in fact the dominant mode of glaciation and produced large increases in relief since ~6 Ma, then the findings of this study should corroborate the hypothesis of Ma et al. (in review).

2. Overview

Deep U-shaped valleys and fjords are common geologic features of the Patagonian Andes [Fig. 2]. This glaciated landscape serves as a natural laboratory for studying how surface processes like glaciation have affected the local topography over geologic time, in particular in the last several million years. As the global temperature cooled over the late Cenozoic, glaciers formed and they incised the Patagonian Andes. While dated glacial debris has helped constrain the timing of late Cenozoic glaciation in the Patagonian Andes, the topographic effects of these early glaciations remain poorly understood.

2.1. Glacial erosion and topographic evolution

Broecker and Denton (1989) was first to demonstrate a correlation between the summit elevations of mountain ranges and their corresponding snowline elevations or equilibrium level altitudes (ELAs) [Fig. 3]. The original observation of this correlation was presented in Skinner and Porter (1987). The authors hypothesized that the downward sloping north-south axis of the Andes was due to colder temperatures at higher latitudes giving rise to erosive glaciers that eroded the orogen fast enough to limit mountain height and growth more in the southern half of the range than the northern half. This idea was popularized when Broecker and Denton (1989) closely fit the trend line of the modern summit elevations of the western cordilleran ranges of N. and S. America with that of the modern and LGM ELAs for the ranges. The established correlation between summit elevation and mean long-term ELA suggested that glacial erosion might in fact be a controlling factor in the height and shape of mountain belts like the Andes.

Figure 2. View of U-shaped valley and Baker River from the southern highway in Patagonia (photo by Ryan Laemel).

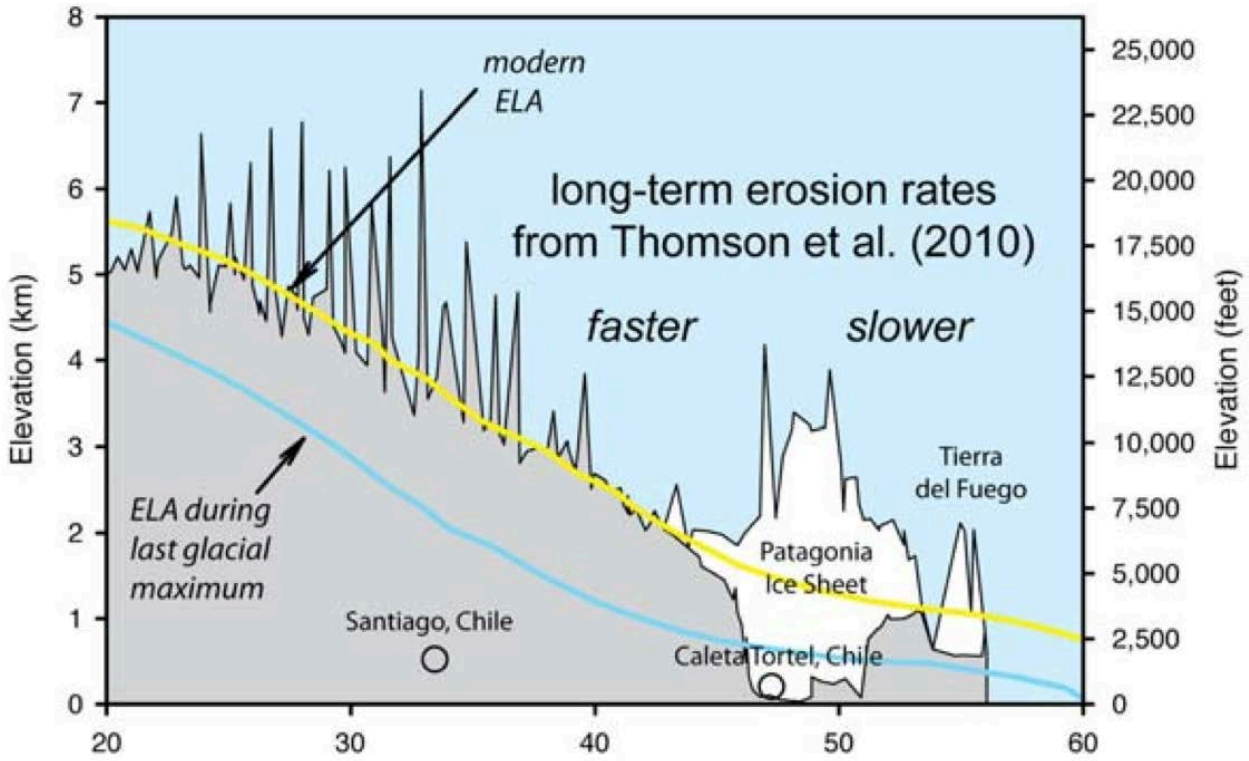

Figure 3. Cross-section of elevation in the Andes with modern and LGM ELAs superimposed to show correlation between summit height and ELA, evidence of the glacial buzzsaw (after Skinner and Porter, 1987; Broecker and Denton, 1989).

Brozovic et al. (1997) provided evidence from the Himalaya supporting the hypothesis that glacial erosion might be a limiting factor in topographic evolution. This theory came to be known as the glacial buzzsaw hypothesis (Brozovic et al., 1997; Montgomery et al., 2001; Mitchell and Montgomery, 2006; Foster et al., 2008; Egholm, 2009). A study conducted in the northern Patagonian Andes (Thomson, 2002) also showed a correlation between summit elevation and ELA despite variable uplift rates in the late Cenozoic. However, Egholm et al. (2009) discovered that the summit elevations in the central and southern Patagonian Andes were significantly higher than the mean long-term ELA, contradicting the belief that the glacial buzzsaw was active along the entire length of the Patagonian Andes. The conflicting results of Thomson (2002) and Egholm et al. (2009) suggested there might be a north-south disparity in or latitudinal correlation to the relationship of glacial erosion and topographic evolution. While Ramos et al. (2005) proposed this disparity might be a result of tectonics, the southward decrease in ELA implies there may be a link between glaciation and relief reduction in the Andes.

That said, Molnar and England (1990) and Peizhen et al. (2001) found that late Cenozoic global cooling was accompanied by not only increased erosion rates but also increases in topographic relief [Fig. 4], especially for large tectonically active mountain belts like the Andes. Studies of the Patagonian Andes (Thomson et al., 2010; Ma et al., in review) have corroborated their conclusions. How glacial erosion affects topographic evolution in the Patagonian Andes, however, remains uncertain and thus demands further study of glaciation and relief change.

2.2. Quantifying relief change from (U-Th)/He thermochronometry

Thermochronology, a technique for dating the thermal history of specific minerals, can be used to quantify the timing of rock exhumation. Low temperature thermochronology can offer insight into how surface processes like glaciation affect landscape evolution. Most methods of thermochronometry rely on the relative measurement of the reactants and products of a radioactive decay reaction in a particular mineral to determine the time at which that mineral passed through a specific temperature in the earth's crust and cooled; in doing so, the diffusive loss of radioactive decay products relative to their formation loss is slowed and thus allows the products to accumulate in the host mineral (Braun, 2006). Typically one isotope, known as the daughter isotope, is produced by the radioactive decay of a naturally occurring unstable isotope,

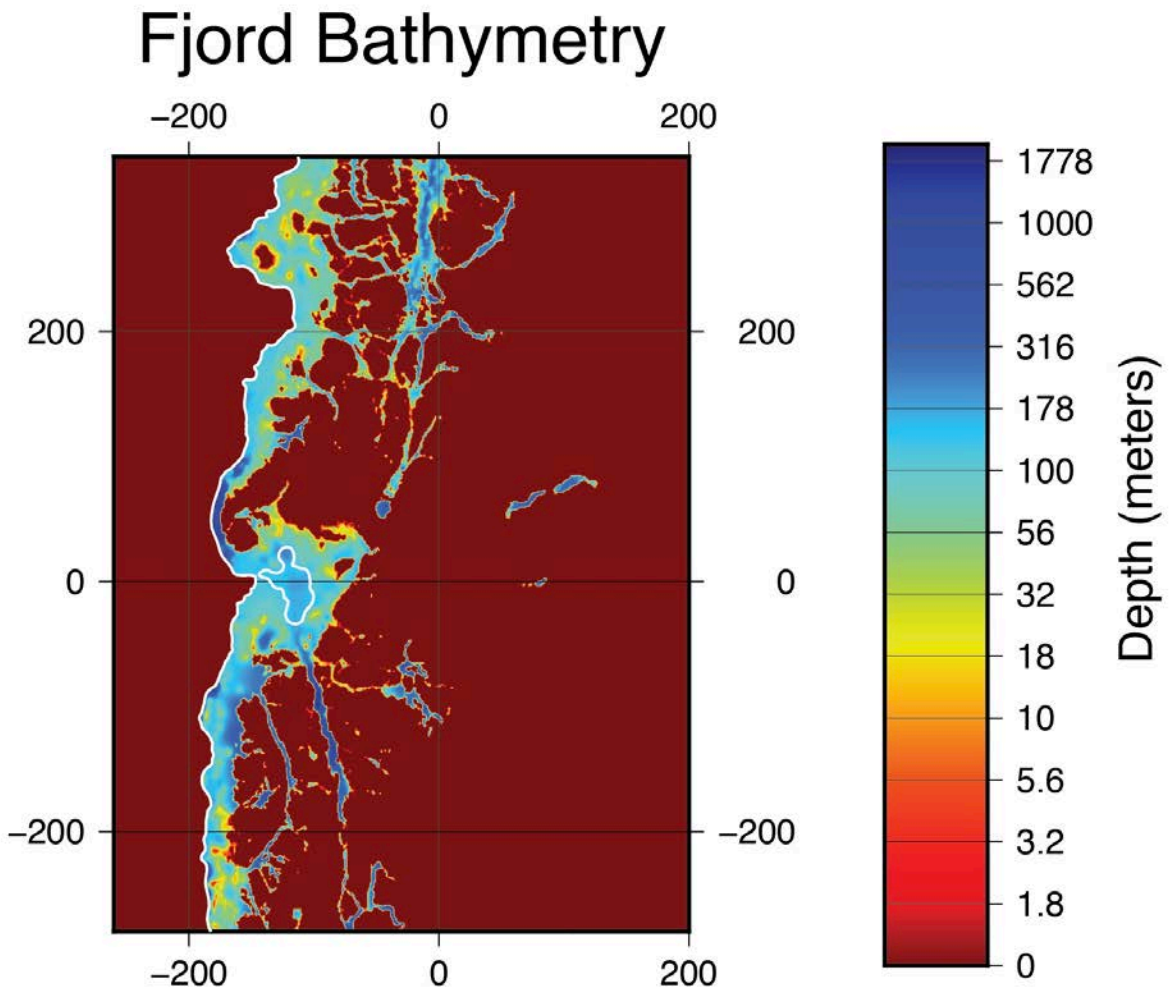

Figure 4. 400 square km area of the central Patagonian Andes showing deep fjords and glacial overdeepenings, e.g. Canal Messier (~48°S, ~75°W) exceeds 1200 m in depth; these features are testaments to the high local topographic relief observed along the mountain belt.

referred to as the parent isotope, present in a mineral within a rock matrix. The cooling age provided by a thermochronometer is calculated from the relative abundances of the parent and daughter isotopes present in the mineral [Fig. 5] (Braun, 2006). Therefore, to obtain the age of a sample, the present day abundances of its parent and daughter isotopes must be measured.

For the apatite (U-Th)/He thermochronometer, which is a system commonly used to date the thermal history of rocks in glaciated landscapes, the relative abundances of U, Th, and He are measured to determine the age of a sample. In the apatite (U-Th)/He system, He, the daughter isotope, is produced in its gaseous state from the alpha decay of its parent isotopes, which include U-235, U-238 and Th-232. He is extracted from the sample by heating in either a vacuum-sealed furnace or a laser cell at temperatures below those at which grain melting or fracture occurs (Farley, 2002). After gas is expelled from the mineral grain, its He content is measured using a noble gas mass spectrometer (Farley, 2002). What is left of the mineral grain is dissolved, forming a solution containing the U and Th parent isotopes that are measured using inductively coupled plasma mass spectrometry (Farley, 2002). By first extracting the He gas and then dissolving the rest of the sample, the abundances of the U and Th parent isotopes can be measured from the same grain as the He daughter isotope, eliminating any issues associated with grain heterogeneity (Farley, 2002; Braun, 2006).

Rutherford (1907) and Soddy (1914) were first to propose that the production of He from U and Th decay provided a way of computing the "age" of a rock. At a time when geoscientists cared only for absolute ages, as they were trying to pin down the age of Earth, the apatite (U-Th)/He system, which produced consistently younger ages than those calculated using the U-Pb system, was deemed an unreliable thermochronometer (Holmes, 1913; Hurley et al., 1956). However, geoscientists failed to recognize until the late twentieth century that because He diffuses easily out of the mineral lattice at lower temperatures, its age measurements not only should be younger than those calculated using higher temperature systems but also can be used to describe the vertical motions of rocks over time and, unlike high temperature chronometers, they can be used to determine how surface processes affect topographic evolution (Braun, 2006).

Today, geoscientists know that by measuring the relative amounts of U, Th, and He in an apatite bearing rock sample, the cooling age of that rock can be calculated. The "cooling" or "apparent" age of a rock differs from its "absolute" age in that the former does not correspond to the formation time of the rock but rather to the time at which the dated rock particle passed

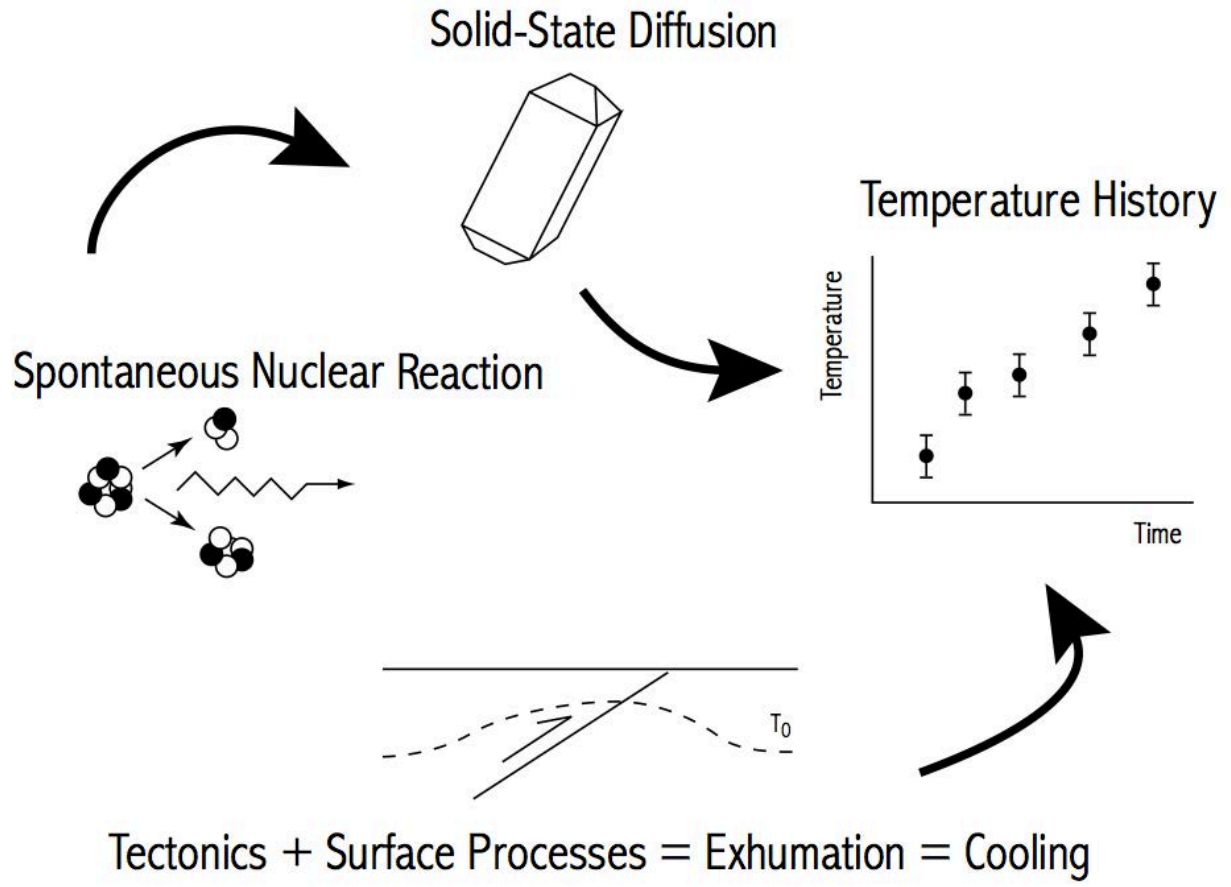

Figure 5. Schematic showing how nuclear decay reactions that occur at known rates in minerals can be used to construct the time-temperature history of a tectonic setting undergoing exhumation and cooling (from Braun, 2006).

through a specific temperature in the earth's lithosphere. Dodson (1973) formally defined this passing point as the "closure temperature." At temperatures above the closure temperature, the system is open and daughter product diffuses more rapidly than it accumulates. Once a mineral passes through the closure temperature, however, it becomes a closed system wherein diffusion is slow in comparison to daughter product production by radioactive decay, allowing the host mineral to build up and retain daughter product (Braun, 2006). Zeitler et al. (1987) proposed that the diffusion of He from apatite could be quantified and that helium-apatite (HEA) ages could be used to constrain the cooling histories of rocks through low temperature "isotherms" or lines of equal temperature.

Diffusion experiments such as Wolf et al. (1996) and Farley (2000) demonstrated that the apatite (U-Th)/He system is sensitive to temperatures as low as 40°C with closure occurring around 70°C; however, it was shown that the closure temperature depends on both the cooling rate and mineral grain size. In the central and southern Patagonian Andes, where low erosion rates have been observed, the apatite (U-Th)/He thermochronometer has a low closure temperature of about 62°C; this value corresponds to a depth of approximately 2-3 km given the geothermal gradient of the region (Reiners and Brandon, 2006).

In the earth's upper crust, isotherms tend to mimic surface features; that is, near surface isotherms are muted forms of the topography at the surface [Fig. 6]. The degree to which an isotherm mimics topography decreases exponentially with depth (Turcotte and Schubert, 1982). Thus low temperature thermochronometers, having shallow closure surfaces, best record changes in topography caused by surface processes (Braun, 2006). McPhillips and Brandon (2010) introduced the term "isochrone," or a surface for which all points are of the same cooling age, to illustrate this link between cooling ages and topographic evolution. Isochrones can be mapped at the surface to generate a set of equal age surfaces that resemble a mapped stratigraphic sequence. Isochrones thus relate thermal and structural information in an intelligible way.

Because low temperature thermochronometric systems, e.g. apatite (U-Th)/He, have shallow isotherms that mimic the shape of the topography at the surface, they are often used to quantify the effects of surface processes like glaciation on topographic evolution. For example, relief change caused by glacial erosion can be determined and in fact quantified using low temperature thermochronology (Thomson et al., 2010; Valla et al., 2011; Valla et al., 2012; Ma et al., in review). Braun (2002) provided a simple methodology for using age-elevation

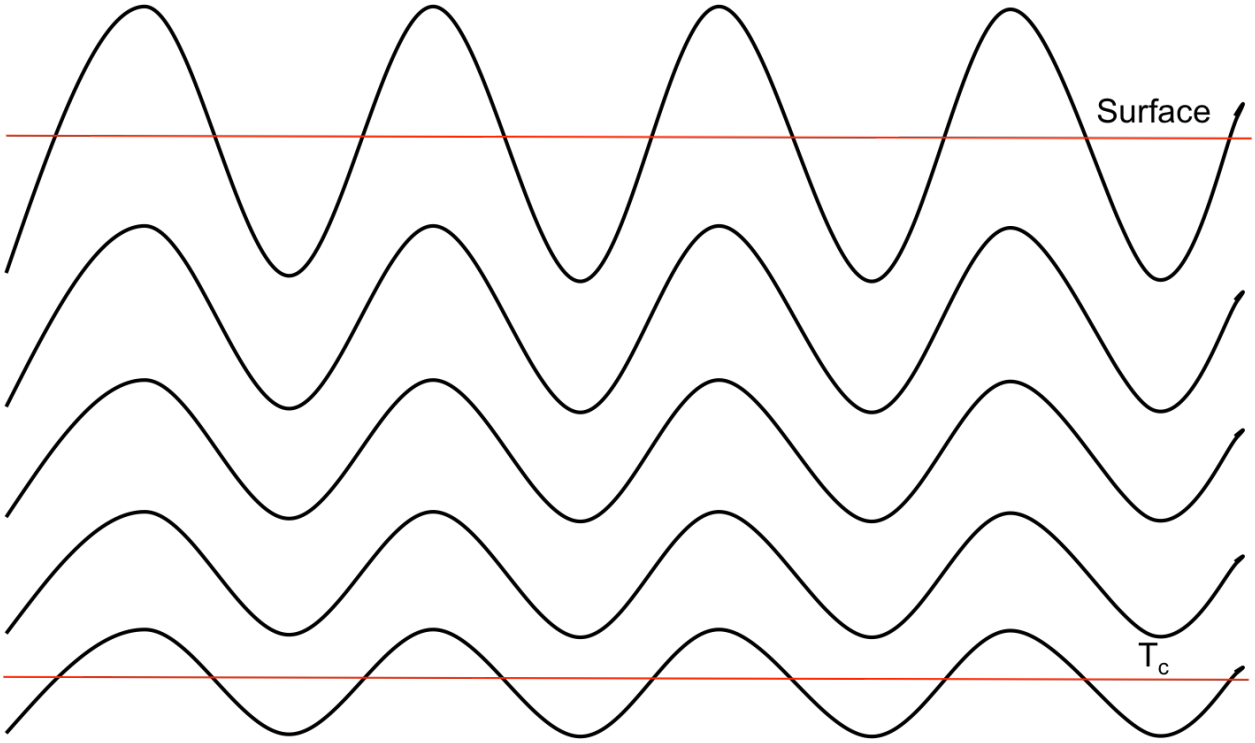

Figure 6. Diagram showing how topography at the surface influences the shape of the isotherms in the subsurface; this perturbation effect decreases exponentially with depth as shown by Turcotte and Schubert (1982); the top and bottom red lines represent the mean surface topography and mean closure surface topography, respectively.

relationships constructed from thermochronologic data to quantify erosion rates and relief change for low temperature systems. This study applies the methods outlined in Braun (2002) to extract information about erosion rates and relief development from a new set of HEA ages collected in the Central Patagonian Andes. All of the existing thermochronometric data for the entire rage are shown in Fig. 7.

2.3. Geologic setting

The Patagonian Andes has experienced mountain building as a result of an increase in the convergence rate of the Nazca and South American plates to ~11-15 cm/y since ~25 Ma according to plate reconstructions from seafloor magnetic anomalies and paleomagnetically dated terrestrial rock samples (Steinmann, 1929; Pardo-Casas and Molnar, 1987; Somoza, 1998). On decadal, centennial and millennial scales, mountains are generally regarded as steady, static masses of rock (Brozovic 1997). On scales of tens of thousands to millions of years, however, mountains may be considered dynamic, as tectonic uplift and surface erosion may combine to exhume many kilometers of rock (Braun, 2006). The balance of tectonic and geomorphic processes governs the growth of mountains.

Using the Patagonian Andes as an example, Thomson et al. (2010) argued that glacial erosion, a geomorphic process, is an important factor in mountain building. Evidence indicates geomorphic erosion has been the main form of denudation since ~25 Ma (Thomson et al., 2001). Fluvial incision and hillslope mass transport, i.e. landslides, were the dominant forms of erosion until glaciation occurred as early as 7 Ma and continued as late as the Last Glacial Maximum, as suggested by the age range of glacial till deposits collected on the east side of the Andes (Mercer and Sutter, 1982; Thomson et al., 2001; Kaplan et al., 2005). Further evidence of glaciation in the Patagonian Andes includes the downward slope of the range along its north-south axis and the presence of fjords and overdeepenings (Skinner and Porter, 1987; Thomson et al., 2001).

While structural variation of the east side of the mountain belt indicates that shortening is an ongoing process within the core of the range, the lack of evidence of fast uplift rates suggests uplift is mostly due to erosion and isostatic rebound, not tectonic forces (Molnar and England, 1990; Peizhen et al., 2001). Ma et al. (in review) provided further evidence of fast erosion rates. The study showed that when glaciation started ~6 Ma, it was in the form of large, highly erosive

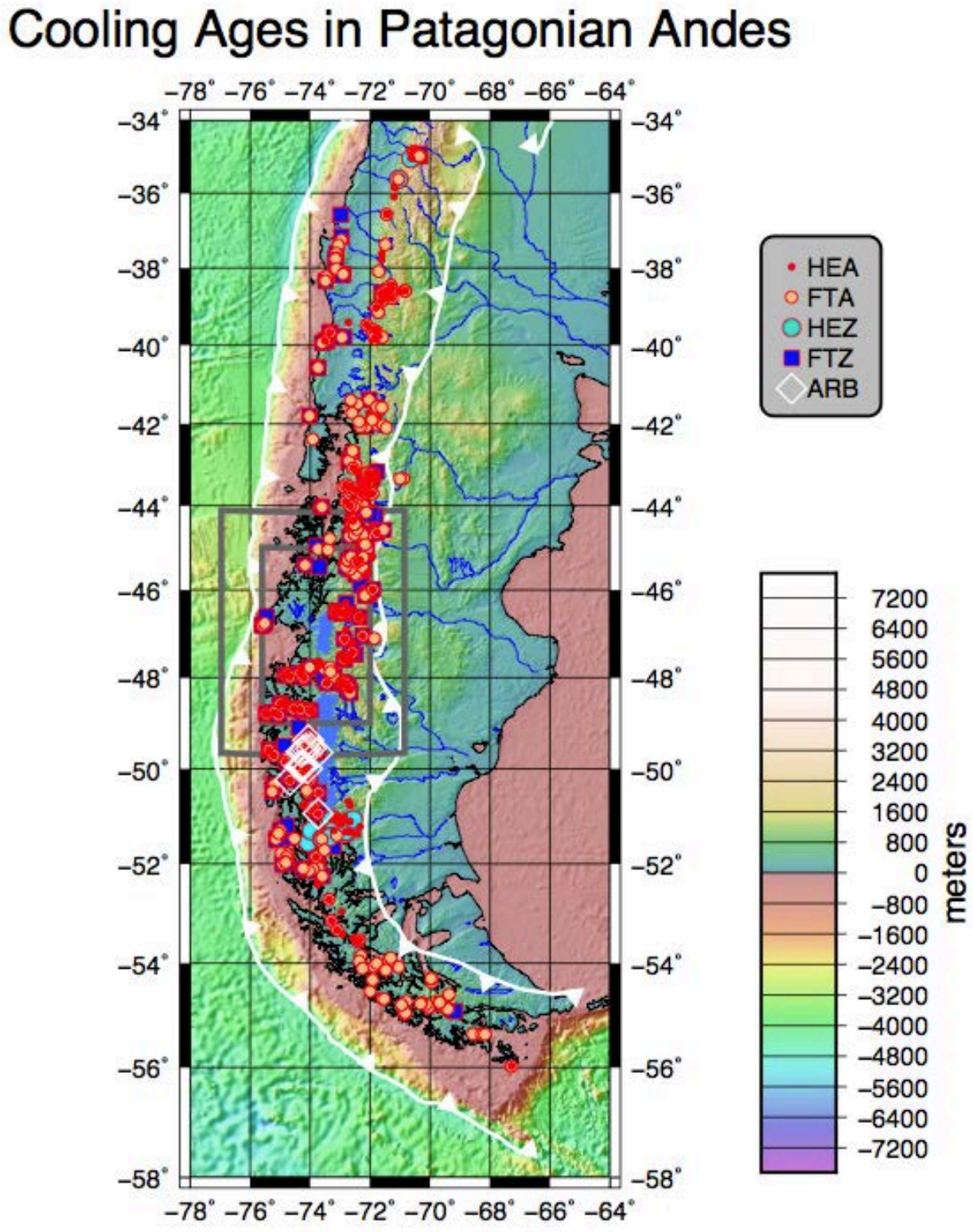

Figure 7. All existing thermochronometric data for the Patagonian Andes.

ice caps that produced substantial increases in regional relief (Ma et al., in review). By using inverse modeling of existing thermochronometric data for the Patagonian Andes, Herman and Brandon (in review) found a 4- to 5-fold increase in the erosion rate of the range from ~6-2 Ma. Fast erosion rates and relief formation in the Patagonian Andes since ~6 Ma suggest the range has been one of the most active geomorphic settings in the world in recent geologic time.

3. Study Area

Recent studies of low temperature thermochronologic data from the Patagonian Andes (Thomson et al., 2001; Thomson et al. 2010; Ma et al., in review) have contributed much to our understanding of the glacial history of the mountain belt. HEA dating is one of the predominant thermochronometric methods used in the Patagonian Andes because it is able to provide information about the effects that surface processes like glaciation have on topographic evolution. The HEA system is also used widely throughout the Patagonian Andes because even though the basement rock is metamorphic phyllite, there is plenty of dateable bedrock in the area due to the presence of the Patagonian batholith, an apatite rich granitic pluton.

When selecting a study area for a thermochronometric study, the mineralogy, geology and accessibility of the sites in question must be assessed. The characteristics needed for a HEA thermochronologic study of glacial erosion and topographic evolution in the Patagonian Andes include: high topography, evidence of glaciation, apatite rich bedrock and accessibility. High topography provides the large range in altitude needed bring a range of ages from the closure surface at depth to the surface where they can be collected. The elevation of a study area can be determined from digital elevation model data.

While many studies have shown that this region is a glaciated landscape, it is important to find local evidence of glaciation, e.g. glacial features and modern ice sheets, near the sampling locations. Apatite rich bedrock is critical to conducting a HEA thermochronometric study because apatite is the mineral used in HEA dating. The collected samples must be in-situ bedrock samples, not loose cobbles, to study the formation of local relief, as cobbles can be transported large distances by glaciers. Accessibility is also an important consideration because vertical transects must be conducted in order to construct age-elevation relationships that are used to quantify erosion rates and changes in relief.

The sampling sites of Fjord Steffen and Cordón Los Ñadis [Fig. 8] were chosen because they meet these requirements. At both sampling locations the apatite rich Patagonian batholith intersects high topography. Glacial features such as fjords, glacial rivers and high relief peaks are present at both sites. In addition, these sites are accessible by car or boat and require low to moderate climbing skills, an important consideration to make when conducting vertical transects of over 1 km in elevation. Other valleys closer to the Northern Patagonian Ice Field exhibit similar features and would make for good study areas. However, many of them are less accessible and require technical mountaineering skills. That said, samples from these areas that are closer to the ice sheet would make valuable additions to the existing thermochronologic dataset for the Patagonian Andes and should be collected in the future.

4. Sampling and Processing

Collecting multiple samples in close geographic proximity to each other is essential to building age-elevation profiles. Sampling vertical transects of mountains that span large ranges in altitude allows for an assessment of timespans during which samples currently located at different elevations passed through the closure isotherm of a given chronometer. We collected 15 samples of ~2-3 kg from the two sampling sites. We found that this mass of Patagonian batholith would yield sufficient apatite for HEA dating.

Standard mineral separation techniques were used to extract apatite grains from the rock matrix. First, samples were broken into ball-sized rock fragments using a sledge. Then samples were crushed into gravel using a Bico chipmunk jaw crusher. Next, samples were run through a Bico disk mill to pulverize gravel-sized rock fragments into coarse sand. The chief concern of this crushing process is over-crushing since broken grains do not provide reliable cooling ages, as they tend to experience daughter and parent product losses (Braun, 2006). For example, if part of the grain were removed, then it would result in a reduction in age.

A mesh sieve and Ro-tap sieving machine were used to ensure the samples met the grain size needed for HEA dating. Next, a shaking table was used to separate them by density. Heavy liquids, i.e. lithium-based tungstate (LST) and methylene iodide (MEI), were used for further density separations. The sample sizes were further reduced using a magnetic barrier Frantz, which uses a controllable electromagnet to eliminate unwanted magnetic grains. The apatites

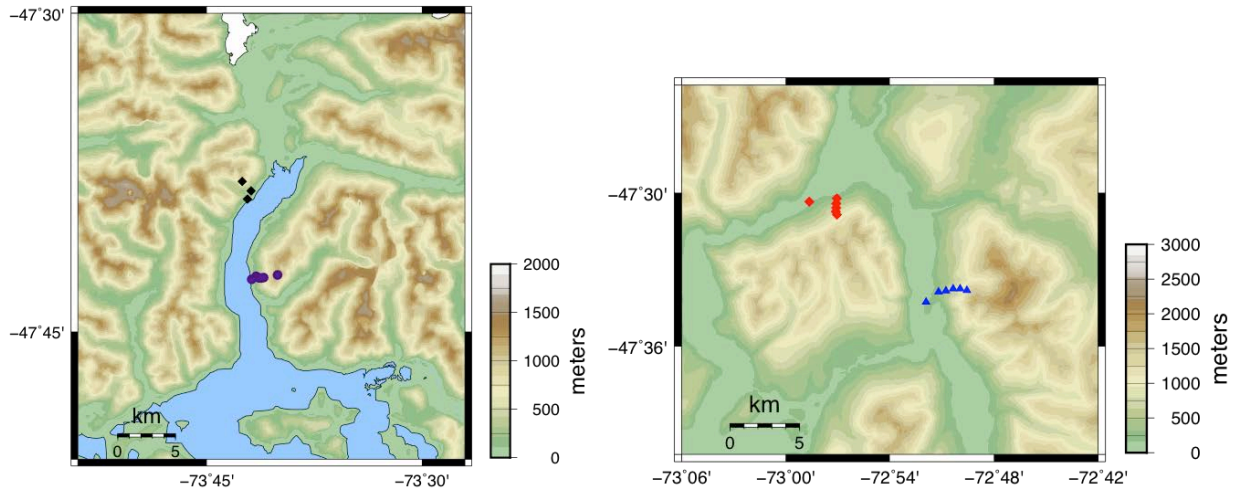

Figure 8. Topographic maps of the two sampling locations, Fjord Steffen (left) and Cordón Los Ñadis (right), in the Patagonian Andes with sample locations superimposed to show vertical transects used to construct age-elevation profiles.

were examined under an Olympic Stereozoom electron microscope. Only high quality, inclusion-free apatite grains [Fig. 9] were picked for analysis. Cooling ages were obtained by measuring the present day abundances of U, Th and He as described in Section 2.2.

5. Methods

Braun (2002) used a schematic of rock exhumation to demonstrate how the perturbation of the closure surface by the topography at the surface and changes in topographic relief not only are recorded in the cooling histories of rocks but also reflected by changes in the slope of the age-elevation relationship constructed from their cooling ages. Considering a closure isotherm with scale factor for its mean amplitude relative to the mean amplitude of the surface topography, assigned the symbol α, and a modern or post-relief change surface topography with a scale factor for its amplitude relative to the amplitude of a past or pre-relief surface topography, assigned a symbol of β, an equation is developed to quantify the effects that vertical scaling of both the amplitude of the closure surface, i.e. a perturbation of the isotherms, and the amplitude of the surface topography, i.e. a change in relief, has on the slope of the age-elevation relationship. Three examples of rock exhumation and cooling are developed to show that this general equation for the slope of the age-elevation relationship derived in Section 5.1 can be used to compute the slope of the age-elevation profiles for each of the three examples. Then this analysis is applied to the study area to estimate erosion rates and relief change in the two sampling sites.

5.1. General equation for the slope of the age-elevation relationship

In the schematic [Fig. 10], the mean amplitude of the closure surface is represented by the straight dashed line at the bottom of the diagram. The closure surface is represented by the dashed curve labeled $T = T_c$ where T_c is defined as the closure temperature of the thermochronometer. The past or pre-relief change surface topography is shown by the dashed curve at the top of the diagram. The mean amplitude of the pre-relief change surface is represented by the straight dashed line at the top of the diagram that intersects the two topographies shown. The amplitude of the closure surface is related to the amplitude of the past

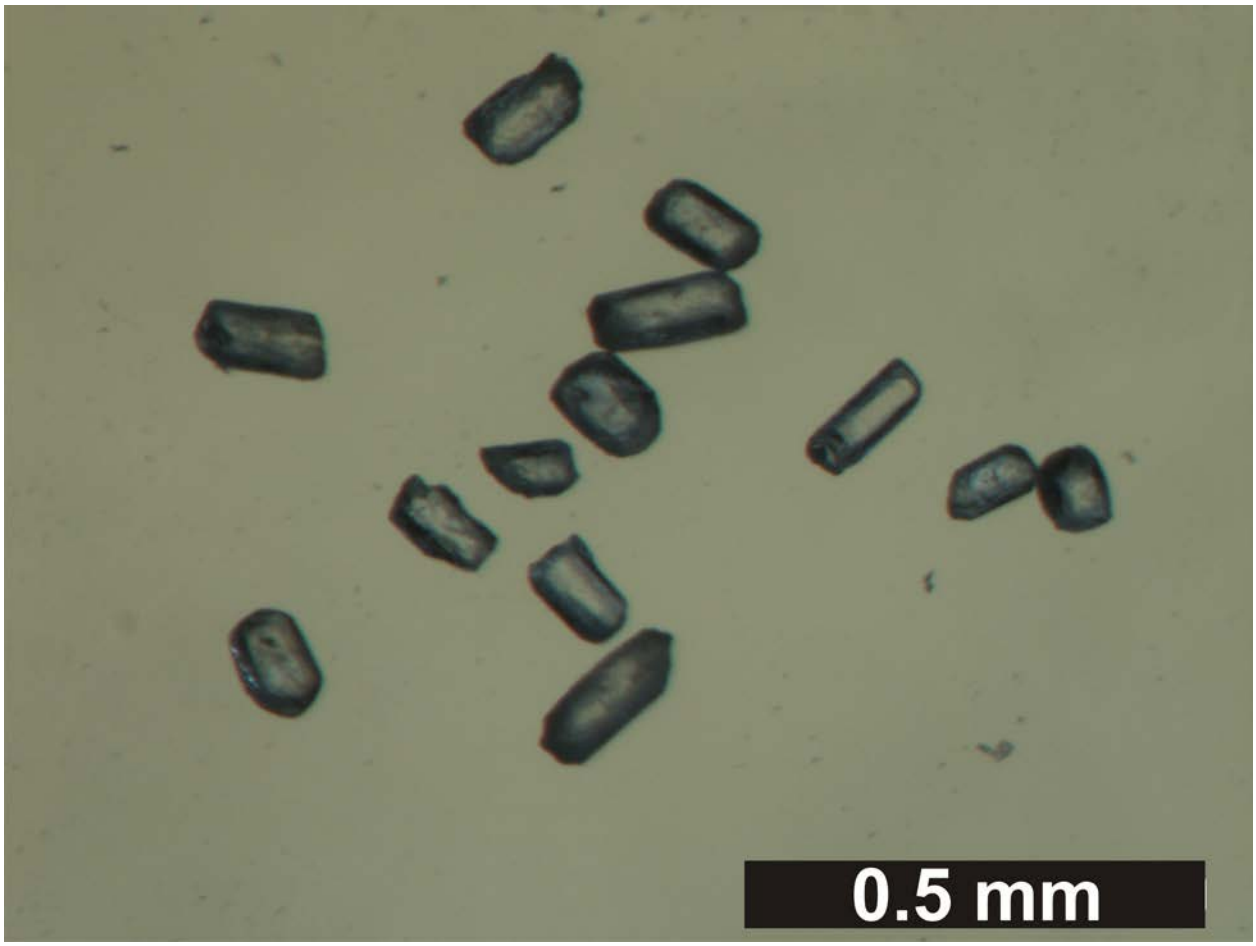

Figure 9. Image of apatite grains taken from an electron microscope (from University of Leicester).

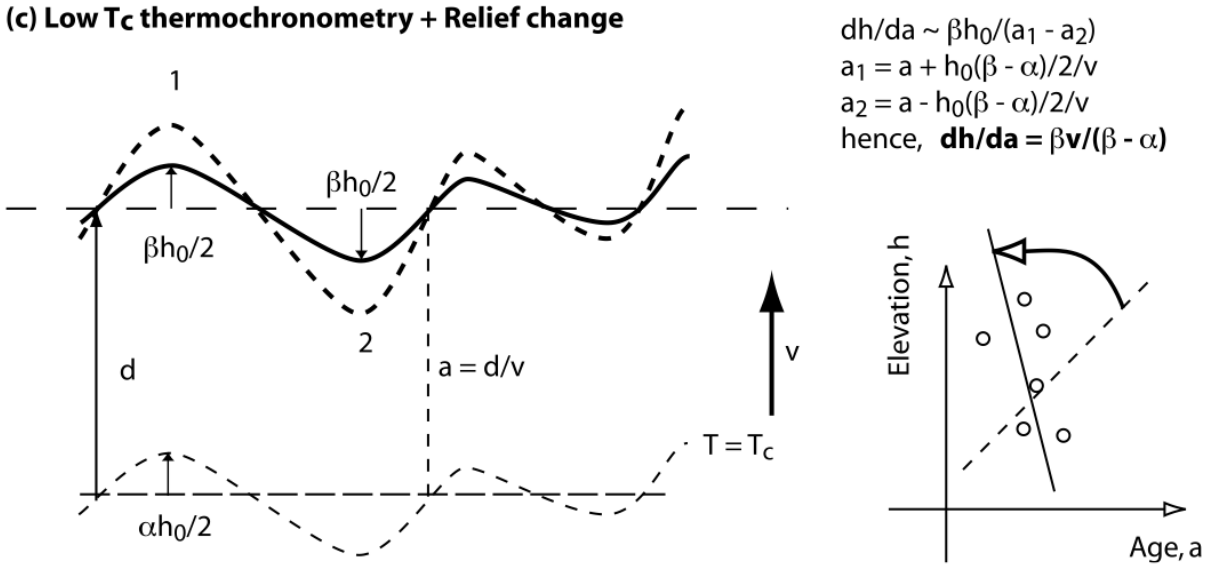

Figure 10. Diagram showing how to construct an age-elevation profile for a set of rock samples that pass through a closure isotherm that mimics the surface topography and a surface topography that has undergone a change in relief; in this case, the slope of the AER is equal to the erosion rate, v, multiplied by the factor $\beta/(\beta-\alpha)$ (from Braun, 2002).

or pre-relief change surface topography by the factor α, which is equal to the ratio of the mean amplitude of the closure surface topography to the mean amplitude of the pre-relief change surface topography. In other words, α is a factor that quantifies the vertical scaling of the amplitude of the closure isotherm relative to the amplitude of the pre-relief change topography. Thus α can be used to quantify the perturbation of the closure surface.

The modern or post-relief change surface topography is represented by the solid curve. The mean amplitude of post-relief change surface is shown by the straight dashed line at the top of the diagram that intersects the topographies. Note that the mean amplitudes of the pre-relief and post-relief change surfaces are equal. Also note that because the mean amplitudes of the pre-relief and post-relief change surfaces are equal, α can be used to express the vertical scaling of the closure surface relative to both topographies. The amplitude of the modern topography is related to the amplitude of the past topography by the factor β, which is equal to the ratio of the amplitude of the post-relief change surface to the amplitude of the pre-relief change surface. In other words, β is a factor that quantifies the vertical scaling of the amplitude of the post-relief change topography relative to the amplitude of the pre-relief change topography. Thus β can be used to quantify the relative relief change experienced by a landscape.

The slope of the age-elevation relationship, dh/da, between points one and two for the post-relief change topography in the diagram is calculated by the ratio of the vertical distance between points one and two to the horizontal difference between points one and two. For the post-relief surface the vertical distance between points one and two is equal to the sum of the amplitudes of points one and two, i.e. βh_0. The horizontal distance between points one and two is equal to the difference between the ages on the post-relief surface at points one and two. The age at any point on the post-relief surface is equal to the distance between the closure isotherm and the surface divided by the erosion rate v. For points one and two on the post-relief surface the ages of points one and two are expressed as:

$$a_1 = a + \frac{h_0(\beta - \alpha)}{2v}$$

$$a_2 = a - \frac{h_0(\beta - \alpha)}{2v}$$

Because the vertical and horizontal distances between points one and two are known, the slope of the age-elevation relationship for the transect between points one and two on the post-relief surface can be calculated. The slope, dh/da, is equal to:

$$\frac{dh}{da} = \frac{\beta v}{\beta - \alpha}$$

This equation can be used as a general equation to calculate the slope of an age-elevation profile for topographies that have perturbed closure surfaces and have experienced relief changes provided that the values for the parameters α, β and v are known. Furthermore, rearranging this equation can allow for the quantification of either α, β or v if the slope of the age-elevation profile, dh/da, and two of the three parameters are known. Thus, this equation can be used to quantify erosion rates and changes in relief from an age-elevation relationship constructed from a thermochronometric dataset collected in the field provided that alpha can be calculated by decomposing the topography into its component wavelengths using a Fourier analysis.

5.2. Case 1: flat closure surface, no relief change

For the first case [Fig. 11] surface topography is represented by the solid black line. The mean amplitude of the surface topography is signified by the dashed line that passes through the surface topography. The closure isotherm is labeled $T = T_c$ where T_c is the closure temperature and is shown by the dashed line at the bottom of the diagram. Because this schematic is drawn for a high temperature thermochronometer, e.g. FTZ or KAr system, it is assumed that the closure surface is uninfluenced by the surface topography and thus is flat. Rock particles are exhumed at a rate v that is equal to the erosion rate. The rocks travel a distance d from the closure surface to the mean amplitude of the surface topography. Age is calculated as the ratio of this distance to the erosion rate and is given by:

$$a = \frac{d}{v}$$

Because the erosion rate is fixed in this diagram and the two to follow, the age depends solely on the distance between the closure surface and the surface topography. Therefore, relatively young ages are observed where the elevation of the surface topography is lower than the mean amplitude of the surface topography, as the distance between the closure surface and the surface is shorter than d, and relatively older ages are observed where the elevation of the surface topography is greater than the mean amplitude of the surface topography, as the distance between the closure surface and the surface is longer than d. Therefore age increases with height because relatively young ages are located at topographic lows and relatively old ages are located

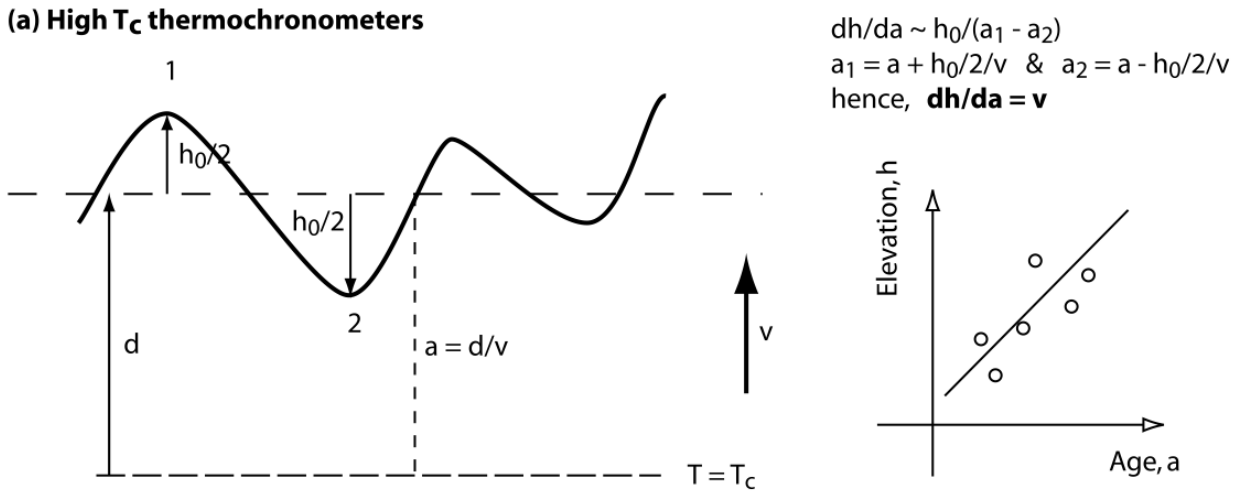

Figure 11. Diagram showing how to construct an age-elevation profile for a set of rock samples that pass through a flat closure isotherm; in this case, the slope of the age-elevation relationship (AER) is equal to the erosion rate, v (from Braun, 2002).

at topographic highs. By selecting samples along the surface topography from point one to point two, an age-elevation profile is constructed. One of the oldest ages in the dataset is observed at point one. Its distance between the closure surface and the mean amplitude of the surface topography is:

$$z = d + \frac{h_0}{2}$$

The age of point one is:

$$a_1 = \frac{d + \frac{h_0}{2}}{v}$$

After simplifying the age of point one is given by the following:

$$a_1 = a + \frac{h_0}{2v}$$

One of the youngest ages in the dataset is observed at point two. Its distance between the closure surface and the mean amplitude of the surface topography is:

$$z = d - \frac{h_0}{2}$$

The age of point two is:

$$a_2 = a - \frac{h_0}{2v}$$

The slope from point one to point two is calculated as the ratio of the vertical distance between points one and two, which is equal to the sum of the amplitudes at each point, to the horizontal distance between points one and two, which is equal to the age difference between the two points. Thus, slope is:

$$\frac{dh}{da} = \frac{h_0}{a_1 - a_2}$$

Inputting the expressions for a_1 and a_2 into the expression above gives the slope of the age-elevation profile:

$$\frac{dh}{da} = \frac{h_0}{\left(a + \frac{h_0}{2v}\right) - \left(a - \frac{h_0}{2v}\right)}$$

After simplifying the slope of the age-elevation profile for Case 1 is:

$$\frac{dh}{da} = v$$

Thus, for the first case, the slope of the age-elevation profile is equal to the erosion rate. This result makes intuitive sense because as rock particles are exhumed through a flat closure surface with a velocity equal to the exhumation rate, the distribution of ages with height is expected to vary linearly with the rate at which the rock particles were transported to the surface. It is no wonder then that for high temperature thermochronometers the slope of a trend line for a plot of age-elevation data tends to provide a good estimate of the erosion rate.

The same result is obtained by using the general equation for the slope of the age-elevation relationship derived in Section 5.1. For a flat closure surface, $\alpha = 0$ because the closure surface has no amplitude and $\beta = 1$ because there is no change in relief. By inputting these values into the general equation for the age-elevation relationship, a slope equal to the erosion rate is obtained.

5.3. Case 2: attenuated closure surface, no relief change

The schematic used in the second case is almost the same as the one used in the first case [Fig. 12] with the exception of the shape of the closure surface. Because the second schematic is drawn for a low temperature thermochronometer, e.g. HEA system, for which the closure surface is shallow, the shape of the closure surface is influenced by the shape of the surface topography. Thus, the closure surface, represented by the dashed curve, mimics the surface topography. The mean amplitude of the closure surface is vertically scaled down from the mean amplitude of the surface topography by a factor of α. As mentioned in Section 2.2 this perturbation effect decreases exponentially with depth. How does this perturbation of the closure surface influence the slope of the age-elevation profile? The effect of changing the shape of the closure surface from a flat surface to one that is a muted form of the surface topography is determined by calculating the slope of the age-elevation profile for this case and comparing it to the slope of the age-elevation profile in Case 1.

For the second case, one of the oldest ages in the dataset is observed at point one. Note that the age observed at point one in the second case is younger than the age observed at point one in the first case because the distance from the closure surface to the surface topography has decreased from Case 1. One of the youngest ages in the dataset is observed at point two. Note that the age observed at point one in the second case is older than the age observed at point one

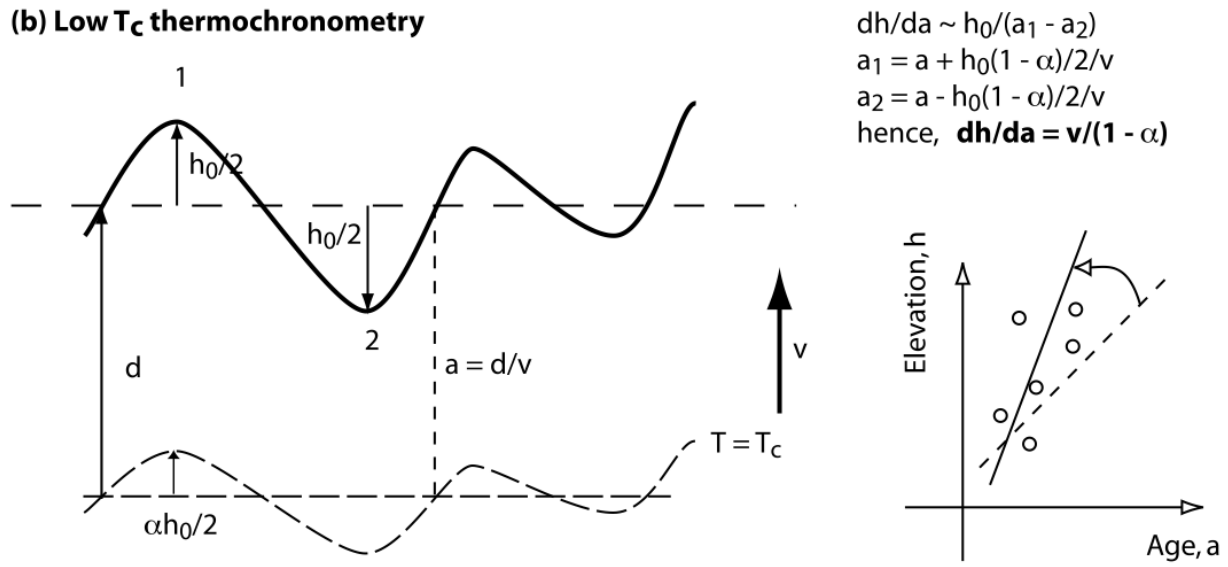

Figure 12. Diagram showing how to construct an age-elevation profile for a set of rock samples that pass through a closure isotherm that mimics the surface topography; in this case, the slope of the AER is equal to the erosion rate, v, multiplied by the factor $1/(1-\alpha)$ (from Braun, 2002).

in the first case because the distance from the closure surface to the surface topography has increased from Case 1. The perturbation effect thus causes a counterclockwise rotation of the trend line of the age-elevation relationship from its position in Case 1 because relatively younger ages appear at higher elevations and relatively older ages appear at lower elevations. Using almost the exact same approach as used in Case 1 with the exception of accounting for the perturbation effect, the slope of the age-elevation profile for Case 2 is:

$$\frac{dh}{da} = \frac{v}{1-\alpha}$$

Thus, for the second case, the slope of the age-elevation profile is equal to the erosion rate, or the slope of the age-elevation profile for Case 1, multiplied by a factor of $1 / (1 - \alpha)$. The perturbation effect experienced by the closure surface is responsible for an increase in the slope of the age-elevation profile and a counterclockwise rotation of the trend line of the age-elevation profile from Case 1. As can be seen by rearranging the slope equation to calculate the erosion rate v, if the age-elevation profile is not corrected for the perturbation effect using α, erosion rates are overestimated by low temperature thermochronometers.

The same result is obtained by using the general equation for the slope of the age-elevation relationship derived in Section 5.1. For a vertically scaled down closure surface with a constant topography, i.e. no change in relief, α is the ratio of the mean amplitude of the closure surface to the mean amplitude of the surface topography and $\beta = 1$ because there is no change in relief. By inputting in these values into the general equation for the age-elevation relationship, a slope equal to the erosion rate multiplied by the factor $1 / (1 - \alpha)$ is obtained.

5.4. Case 3: attenuated closure isotherm, decrease in relief

The same diagram used in the third case is used in the second case [see Fig. 10] with the exception of a change in the shape of the surface topography. The modern or post-relief change topography is represented by the solid curve. The past or pre-relief change topography is represented by the dashed curve. The amplitude of the post-relief surface is vertically scaled down from the amplitude of the pre-relief surface by a factor of β. How does this transition from a past topography with higher relief to a modern one with lower relief change the slope of the age-elevation profile? The effect of decreasing the relief of the topography is determined by

calculating the slope of the age-elevation profile for this case and comparing it to the slope of the age-elevation profile in Case 2.

The age observed at point one in this case is younger than the ages observed at point one in the first two cases because the distance from the closure surface to the post-relief change surface topography is shortest of all three cases. The age observed at point two in this case is older than the ages observed at point two in the first two cases because the distance from the closure surface to the modern surface topography is the longest of all three cases. Therefore, the decrease in relief, coupled with the attenuated closure surface, causes a more pronounced counterclockwise rotation of the trend line of the age-elevation relationship from its position in Case 1 than is caused by the effect of a perturbed closure surface alone. In fact, depending on how small the value of β is, the trend line may even overturn and thus a negative slope would be observed. Note that while in this case $\beta < 1$, β can also be greater than or equal to one if a relative increase in relief is observed for the modern topography, i.e. the opposite of Case 3. Thus, if $\beta \geq 1$, then the trend line would be rotated in a clockwise direction. Using almost the exact same approach as used in Case 2 with the exception of accounting for the change, i.e. decrease, in relief, the slope of the age-elevation profile for Case 3 is:

$$\frac{dh}{da} = \frac{\beta v}{\beta - \alpha}$$

This equation is the same as the general equation for the slope of the age-elevation relationship calculated in Section 5.1. Thus, for the third case the slope of the age-elevation profile is equal to the erosion rate multiplied by a factor of $\beta /(\beta - \alpha)$. The decrease in relief is responsible for an increase in the slope of the age-elevation profile and a counterclockwise rotation of the trend line of the age-elevation profile from Case 1, both of which are more pronounced than they were in Case 2. As can be seen by rearranging the slope equation to calculate the erosion rate v, if the age-elevation profile is not corrected for the perturbation effect using α, as well as changes in relief using β, erosion rates are miscalculated from the slopes of age-elevation relationships for low temperature thermochronometers.

To summarize, for high temperature thermochronometers with flatter closure surfaces, erosion rates are accurately determined by simply taking the slope of the age-elevation relationship; however for low temperature thermochronometers with perturbed closure surfaces,

erosion rates can only be calculated accurately by correcting for the perturbation of the isotherms and any changes in relief using the factors α and β.

The methods discussed in Sections 5.1-5.4 demonstrate how changes in relief affect the slope of age-elevation relationships for low temperature thermochronometers. This study has age-elevation relationships for its two sampling locations in the Patagonian Andes. Thus, the methods that have been discussed in Sections 5.1-5.4 are applied in Sections 5.5-5.7 to quantify erosion rates and changes in relief in Fjord Steffen and Cordón Los Ñadis. Specifically, the assumptions and method used in Case 2 from Section 5.3 are applied to evaluate the age-elevation profiles of Fjord Steffen and Cordón Los Ñadis and estimate erosion rate in each area. If this process does not provide reasonable results for the site in question, then the assumptions and method used in Case 3 from Section 5.4 are applied.

5.5. Calculation of erosion rate v for Fjord Steffen

First, the erosion rate v for the study area is computed using a rearranged version of the general equation for the slope of age-elevation relationships derived in Section 5.1. By decomposing the topography into its component wavelengths using a Fourier analysis, each with its own α value, an average α is calculated for the two sampling locations, which we use in the determination of the erosion rate. By using a least square fit to calculate the slopes of the trend lines for the age-elevation profiles constructed from our data and select data from two other studies (Thomson et al., 2010; Guillaume et al., 2013) [Fig. 13], dh/da is calculated for the two sites, the values of which we use in the calculation of the erosion rate. To calculate the erosion rate from the general equation for the slope of age-elevation relationships from Section 5.1, we set β = 1 to end up with one equation and one unknown, which can be solved; otherwise there would be one equation and two unknowns, which cannot be solved. By inputting the computed values for dh/da and α and assuming β = 1, we calculate the erosion rate v:

$$\frac{dh}{da} = \frac{\beta v}{\beta - \alpha}$$

$$v = \frac{dh}{da}(1 - \alpha)$$

$$v = \left(3.3\frac{km}{m.y.}\right)(1 - 0.32)$$

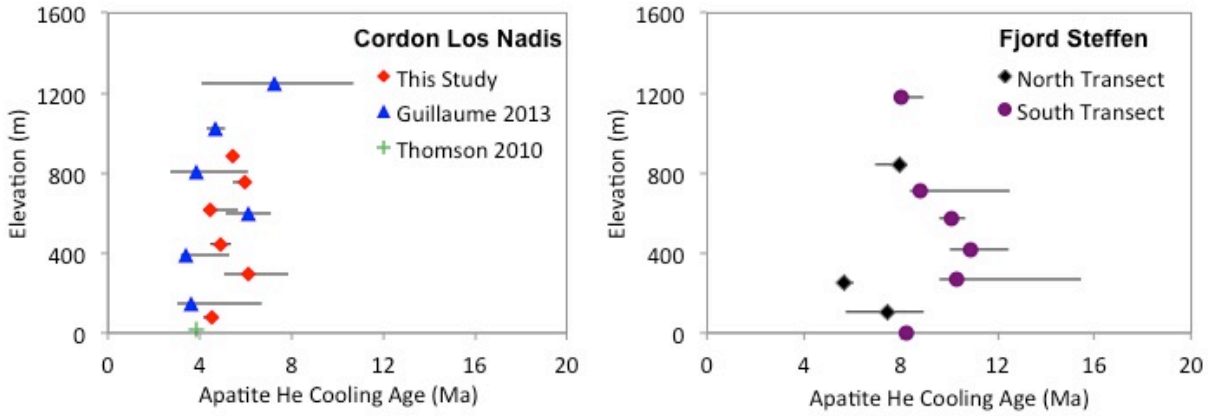

Figure 13. Age-elevation profiles for sampling locations using 15 mean apatite-helium ages from this study and 7 mean apatite-helium ages from two other studies, Thomson et al. (2010) and Guillaume et al. (2013).

$$v = 2.2 \frac{km}{m.y.}$$

From this analysis, an erosion rate of 2.2 km/m.y. is calculated for Fjord Steffen assuming β = 1. Whether β = 1 is a good assumption can be determined by comparing the computed erosion rate with the regional erosion rate derived by Herman and Brandon (in review) from inverse modeling of all the existing thermochronometric data from the Patagonian Andes. For Fjord Steffen, the erosion rate is 2.2 km/m.y., whereas the regional erosion rate computed by Herman and Brandon (in review) is 0.2-0.4 km/m.y. The fact that the calculated erosion rate is a full order of magnitude off the erosion rate from Herman and Brandon (in review) indicates that the assumption β = 1 is a poor one. Even if the erosion rates were only, say, two to three times higher than the erosion rate from Herman and Brandon (in review), the assumption would still be considered poor, as the presence of many old ages at elevations of ~1 km in the Patagonian Andes is indicative of slower erosion rates on the order of the ones calculated by Herman and Brandon (in review).

5.6. Calculation of initial relief factor β for Fjord Steffen

For Fjord Steffen, β is estimated from general equation for the slope of the age-elevation relationship from Section 5.1 and inputting the known values of dh/da, α and v where v is the erosion rate calculated by Herman and Brandon (in review):

$$\frac{dh}{da} = \frac{\beta v}{\beta - \alpha}$$

$$\beta = \frac{\alpha}{1 - \frac{v}{\frac{dh}{da}}}$$

$$\beta = \frac{0.32}{1 - \left(\frac{\left[0.2 \frac{km}{m.y.}, 0.4 \frac{km}{m.y.}\right]}{3.3 \frac{km}{m.y.}} \right)}$$

$$\beta = [0.34, 0.36]$$

From this secondary analysis β is estimated to be 0.34 to 0.36. Therefore the initial relief is estimated to be three times greater than the modern. In other words, a three times reduction in relief is observed in Fjord Steffen of the Patagonian Andes.

5.7. Calculation of erosion rate v and estimation of β for Cordón Los Ñadis

The analysis presented in Section 5.5 is applied to the Cordón Los Ñadis data. Inputting the known values of dh/da and α and assuming β = 1 the the erosion rate v is calculated:

$$\frac{dh}{da} = \frac{\beta v}{\beta - \alpha}$$

$$v' = \frac{dh}{da}(1 - \alpha)$$

$$v' = \left(0.63 \frac{km}{m.y.}\right)(1 - 0.27)$$

$$v' = 0.46 \frac{km}{m.y.}$$

From this analysis an erosion rate of 0.46 km/m.y. is obtained assuming β = 1. This erosion rate is much lower than the erosion rate calculated in Fjord Steffen. By comparing this erosion rate the regional erosions rate from Herman and Brandon (in review) we can determine if β = 1 is a good assumption for Cordón Los Ñadis. The erosion rate for Cordón Los Ñadis is 0.46 km/m.y. and the regional erosion rate from Herman and Brandon (in review) is 0.2-0.4 km/m.y. The fact that this erosion rate is not only within the same order of magnitude as the erosion rate from Herman and Brandon (in review) but also ~10% of the upper limit of the range calculated by Herman and Brandon (in review) indicates that the assumption of β = 1 is a pretty good one.

6. Results

We present 15 new HEA ages [Appendix] from samples collected at two sites, Fjord Steffen and Cordón Los Ñadis, in the Patagonian Andes. Age-elevation profiles were interpreted according to the methods described in Section 5 to compute erosion rates and determine relief change for the two sampling locations. We report dh/da, α, v and β for Fjord Steffen and Cordón Los Ñadis [Table 1].

Sample Site	dh/da (km/m.y.)	α	v (km/m.y.)	β
Fjord Steffen	3.3	0.32	2.2	0.35
Cordón Los Ñadis	0.63	0.27	0.45	1

7. Discussion

In Fjord Steffen the amplitude of present topography is about 1 km on average. Given an erosion rate of ~0.2-0.4 km/m.y., as per Herman and Brandon (in review), we estimate that β = 0.35. This implies that the amplitude of topography was ~3 km at ~8 Ma, i.e. the age of the isochrones exposed at the surface in Fjord Steffen, and thus that the relief was ~6 km. Because relief on this scale is only observed in the most high relief areas of the world, e.g. the Himalaya, this result is an unlikely but nonetheless plausible scenario of landscape evolution in the Patagonian Andes. Furthermore, considering that other studies (Ma et al., in review) found substantial increases in topographic relief as a result of glacial erosion, the likelihood of a three-fold decrease in relief since ~8 Ma is low.

If the conclusion of Ma et al. (in review), that large ice cap glaciations produced significant increase in topographic relief since ~6 Ma, applies in this area, then our estimate of β in Fjord Steffen would be an underestimate. Many factors may have contributed to an underestimate of β in Fjord Steffen. One source of error could be from the large amount of scatter in the ages. For example, if the actual slope, dh/da, of the age-elevation profile for Fjord Steffen were in fact less than slope we calculated, then β would be higher. Another possible factor is that the actual erosion rate may be higher than the erosion rate we used from Herman and Brandon (in review). If the actual erosion rate v for Fjord Steffen were in fact higher than the erosion rate used from Herman and Brandon (in review), then β would also be higher; however, this seems highly unlikely given that Herman and Brandon (in review) uses all existing thermochronometric data from the region to calculate the erosion rate. Finally, if α were in fact lower that the α calculated from the Fourier analysis, then β would be higher as well; however, this too seems unlikely. Thus there are three separate factors, i.e. dh/da, v and α, any or all of which may have led to an underestimate of β.

Possible errors and uncertainty associated with the β calculated in Fjord Steffen suggests a need for statistical analysis of the parameters involved in the calculation of β. A correlational analysis such as a R^2 test could be used to determine which variables correlate most significantly with β. Furthermore, the possibility that ridges have eroded faster than valleys may have led to an underestimate of β. Samples from peaks above fjords and fjord walls would be helpful in determining whether this is the case. Finally, the approach laid out in Section 5 does not account for the lateral propagation of features, as it treats landforms as stationary. The assumption that rock motion occurs only in the vertical certainly has an effect on the age-elevation profiles and their slopes and thereby the calculations of erosion rates and relief changes using those age-elevation relationships.

The above discussion is not, however, to suggest that the results for Fjord Steffen are not valid or conclusive, as these results may in fact accurately quantify the relief change in the Fjord Steffen region. Glaciers have been shown to decrease relief in areas (Willet, 1999; Whipple and Meade, 2006; Tomkin and Roe, 2007). Rather, it serves to point out that the results for Fjord Steffen conflict with the findings of Ma et al. (in review) in that we report a nearly three-fold relative relief decrease in Fjord Steffen, whereas Ma et al. (in review) found large increases in relief in the Patagonian Andes. Thus, we reason that the results for Fjord Steffen are an unlikely but nonetheless plausible scenario of topographic evolution in this region. We recommend further study of how relief development may occur and vary widely on small, local scales in the Patagonian Andes.

In Cordón Los Ñadis the amplitude of present topography is also about 1 km on average. Given an erosion rate of ~0.2-0.4 km/m.y., as per Herman and Brandon (in review), we estimate that $\beta = 1$. This implies that the amplitude of topography was the same at ~4-6 Ma, i.e. the age of the isochrones exposed at the surface in Cordón Los Ñadis, as it is today. In other words, there has been no change in relief since the onset of glaciation. The constant relief observed in Cordón Los Ñadis is also an unlikely but nonetheless plausible scenario of landscape evolution in the Patagonian Andes because it shows no change in relief since the onset of glaciation at ~6 Ma, which also disagrees with the conclusion of Ma et al. (in review). Possible errors and uncertainty associated with the results for Cordón Los Ñadis also suggest a need for statistical analysis of the parameters involved in the calculation of β and the possibilities of a disparity in ridge-valley relief change and erosion as well as the effects of laterally propagating features.

We conclude that the pre-glacial topography of the Patagonian Andes had either the same or higher relief than the modern topography and valley depth has not increased since the onset of glaciation. Although the results of this study conflict with the findings of other studies conducted in the region, it shows that while the glacial buzzsaw is thought to control the topographic evolution of the entire mountain belt, relief development may occur on smaller, more local scales and vary widely along the length of the range.

The fact that different thermochronologic datasets and methods have produced conflicting opinions on how glaciers erode the landscape and enhance relief in the Patagonian Andes suggests that a better understanding of the dynamic between glacial erosion and the formation of relief is needed and we recommend further studies.

8. Acknowledgements

This study was made possible with the financial support of the Karen L. Von Damm '77 Research Fellowship in Geology and Geophysics, the Yale College Dean's Research Fellowship, and the Mellon Fund. First, I thank each of the aforementioned donors for sponsoring this research project and the individuals on their grant approval committees. Second, I express my thanks to Dr. Mark Brandon, whose patience and guidance, uncanny propensity to simplify problems, and cheerful demeanor allowed me to experience the scientific method first hand and apply it to a complex geologic problem. Third, I send my thanks to PhD Candidate Elizabeth Christeleit, whose focus, ability to distill complex concepts into a few succinct and intelligible points, and intimate knowledge of the Patagonian Andes and geomorphology taught me how to conduct a geologic study from start to finish, a process that has been even more challenging and rewarding than I once thought learning how to successfully drive of our standard rental truck from the parking lot of the airport at Puerto Montt, Chile along the meandering and perilous southern highway of Patagonia to our field sites was. Finally, I thank my fellow undergraduate researcher, Wendy DeWolf, for getting me involved with this project in the first place.

9. References

Anders, Alison M., Sara Gran Mitchell, and Jonathan H. Tomkin. "Cirques, peaks, and precipitation patterns in the Swiss Alps: Connections among climate, glacial erosion, and topography." *Geology* 38.3 (2010): 239-242.

Braun, Jean. "Quantifying the effect of recent relief changes on age–elevation relationships." *Earth and Planetary Science Letters* 200.3 (2002): 331-343.

Braun, Jean, Peter Van Der Beek, and Geoffrey Batt. *Quantitative thermochronology: numerical methods for the interpretation of thermochronological data*. Cambridge University Press, 2006.

Broecker, Wallace S., and George H. Denton. "The role of ocean-atmosphere reorganizations in glacial cycles." *Geochimica et Cosmochimica Acta* 53.10 (1989): 2465-2501.

Brozović, Nicholas, Douglas W. Burbank, and Andrew J. Meigs. "Climatic limits on landscape development in the northwestern Himalaya." *Science* 276.5312 (1997): 571-574.

Dodson, Martin H. "Closure temperature in cooling geochronological and petrological systems." *Contributions to Mineralogy and Petrology* 40.3 (1973): 259-274.

Egholm, D. L., et al. "Glacial effects limiting mountain height." *Nature* 460.7257 (2009): 884-887.

England, Philip, and Peter Molnar. "Surface uplift, uplift of rocks, and exhumation of rocks." *Geology* 18.12 (1990): 1173-1177.

Farley, K. A. "Helium diffusion from apatite: General behavior as illustrated by Durango fluorapatite." *Journal of Geophysical Research: Solid Earth (1978–2012)* 105.B2 (2000): 2903-2914.

Farley, Kenneth A. "(U-Th)/He dating: Techniques, calibrations, and applications." *Reviews in Mineralogy and Geochemistry* 47.1 (2002): 819-844.

Foster, David, Simon H. Brocklehurst, and Rob L. Gawthorpe. "Small valley glaciers and the effectiveness of the glacial buzzsaw in the northern Basin and Range, USA." *Geomorphology* 102.3 (2008): 624-639.

Guillaume, Benjamin, et al. "Dynamic topography control on Patagonian relief evolution as inferred from low temperature thermochronology." *Earth and Planetary Science Letters* 364 (2013): 157-167.

Holmes, Arthur. *The age of the Earth*. Harper & Brothers, 1913.

Hurley, Patrick M. "DIRECT RADIOMETRIC MEASUREMENT BY GAMMA-RAY SCINTILLATION SPECTROMETER PART I: URANIUM AND THORIUM SERIES IN EQUILIBRIUM." *Geological Society of America Bulletin* 67.4 (1956): 395-404.

Kaplan, Michael R., et al. "Cosmogenic nuclide chronology of pre-last glacial maximum moraines at Lago Buenos Aires, 46 S, Argentina." *Quaternary Research* 63.3 (2005): 301-315.

McPhillips, Devin, and Mark T. Brandon. "Using tracer thermochronology to measure modern relief change in the Sierra Nevada, California." *Earth and Planetary Science Letters* 296.3 (2010): 373-383.

Mercer, J. H., and John F. Sutter. "Late Miocene—earliest Pliocene glaciation in southern Argentina: implications for global ice-sheet history." *Palaeogeography, Palaeoclimatology, Palaeoecology* 38.3 (1982): 185-206.

Meigs, Andrew, and Jeanne Sauber. "Southern Alaska as an example of the long-term consequences of mountain building under the influence of glaciers." *Quaternary Science Reviews* 19.14 (2000): 1543-1562.

Mitchell, Sara Gran, and David R. Montgomery. "Influence of a glacial buzzsaw on the height and morphology of the Cascade Range in central Washington State, USA." *Quaternary Research* 65.1 (2006): 96-107.

Montgomery, David R., Greg Balco, and Sean D. Willett. "Climate, tectonics, and the morphology of the Andes." *Geology* 29.7 (2001): 579-582.

Pardo-Casas, Federico, and Peter Molnar. "Relative motion of the Nazca (Farallon) and South American plates since Late Cretaceous time." *Tectonics*6.3 (1987): 233-248.

Peizhen, Zhang, Peter Molnar, and William R. Downs. "Increased sedimentation rates and grain sizes 2–4 Myr ago due to the influence of climate change on erosion rates." *Nature* 410.6831 (2001): 891-897.

Ramos, Victor A., and Andrés Folguera. "Tectonic evolution of the Andes of Neuquén: constraints derived from the magmatic arc and foreland deformation." *SPECIAL PUBLICATION-GEOLOGICAL SOCIETY OF LONDON* 252 (2005): 15.

Reiners, Peter W., and Mark T. Brandon. "Using thermochronology to understand orogenic erosion." *Annu. Rev. Earth Planet. Sci.* 34 (2006): 419-466.

Rutherford, E. "Some cosmical aspects of radioactivity." *Journal of the Royal Astronomical Society of Canada* 1 (1907): 145.

Skinner, Brian, and S. Porter. "Physical geology." (1987).

Soddy, Frederick. *The Chemistry of the Radio-elements*. Longmans, Green and co., 1914.

Somoza, R. "Updated azca (Farallon)—South America relative motions during the last 40 My: implications for mountain building in the central Andean region." *Journal of South American Earth Sciences* 11.3 (1998): 211-215.

Steinmann, Gustav, et al. "Geologie von Peru." (1929).

Thomson, Stuart N., Francisco Hervé, and Bernhard Stöckhert. "Mesozoic‐Cenozoic denudation history of the Patagonian Andes (southern Chile) and its correlation to different subduction processes." *Tectonics* 20.5 (2001): 693-711.

Thomson, Stuart N. "Late Cenozoic geomorphic and tectonic evolution of the Patagonian Andes between latitudes 42 S and 46 S: An appraisal based on fission-track results from the transpressional intra-arc Liquiñe-Ofqui fault zone. "*Geological Society of America Bulletin* 114.9 (2002): 1159-1173.

Thomson, Stuart N., et al. "Glaciation as a destructive and constructive control on mountain building." *Nature* 467.7313 (2010): 313-317.

Tomkin, Jonathan H., and Gerard H. Roe. "Climate and tectonic controls on glaciated critical-taper orogens." *Earth and Planetary Science Letters* 262.3 (2007): 385-397.

Turcotte, D. L., and G. Schubert. "Geodynamics: Applications of continuum physics to geological problems." (1982).

Valla, Pierre G., David L. Shuster, and Peter A. van der Beek. "Significant increase in relief of the European Alps during mid-Pleistocene glaciations." *Nature geoscience* 4.10 (2011): 688-692.

Valla, Pierre G., et al. "Late Neogene exhumation and relief development of the Aar and Aiguilles Rouges massifs (Swiss Alps) from low‐temperature thermochronology modeling and 4He/3He thermochronometry." *Journal of Geophysical Research: Earth Surface (2003–2012)* 117.F1 (2012).

Whipple, Kelin X., and Brendan J. Meade. "Orogen response to changes in climatic and tectonic forcing." *Earth and Planetary Science Letters* 243.1 (2006): 218-228.

Willett, Sean D. "Orogeny and orography: The effects of erosion on the structure of mountain belts." *Journal of Geophysical Research: Solid Earth (1978–2012)* 104.B12 (1999): 28957-28981.

Wolf, R. A., K. A. Farley, and L. T. Silver. "Helium diffusion and low-temperature

thermochronometry of apatite." *Geochimica et Cosmochimica Acta* 60.21 (1996): 4231-4240.

Zachos, James, et al. "Trends, rhythms, and aberrations in global climate 65 Ma to present." *Science* 292.5517 (2001): 686-693.

Zeitler, P. K., et al. "U-Th-He dating of apatite: A potential thermochronometer." *Geochimica et Cosmochimica Acta* 51.10 (1987): 2865-2868.

10. Appendix

10.1. Table of apatite (U-Th)/He ages used for this study

Sample name	Latitude	Longitude	Elevation	Age of Weighted Average (Not including highlighted ages)	Standard Err (Ma)	Min Age	Max Age	LowErrBar	HighErrBar	Location
FS16	47.70908	73.69784	0	8.23	0.14	8.07	8.39	0.16	0.16	Fjord Steffen Southern Transect
FS14	47.70662	73.69276	267	10.28	0.10	9.62	15.45	0.66	5.17	Fjord Steffen Southern Transect
FS13	47.70799	73.68935	417	10.89	0.10	10.04	12.46	0.85	1.57	Fjord Steffen Southern Transect
FS12	47.70814	73.68685	573	10.09	0.07	9.60	10.70	0.49	0.61	Fjord Steffen Southern Transect
FS11	47.70767	73.68395	709	8.79	0.05	8.38	12.50	0.41	3.71	Fjord Steffen Southern Transect
FS08	47.70565	73.66784	1175	8.00	0.08	7.86	8.94	0.14	0.94	Fjord Steffen Southern Transect
FS06	47.63965	73.69865	251	5.67	0.05	5.51	6.05	0.16	0.38	Fjord Steffen Northern Transect
FS02	47.63228	73.70897	842	7.92	0.09	6.97	8.03	0.95	0.11	Fjord Steffen Northern Transect
FS17	47.64607	73.70287	105	7.42	0.13	5.75	8.97	1.67	1.55	Fjord Steffen Northern Transect
CLN07	47.5059	72.97732	78	4.52	0.06	4.18	4.63	0.34	0.11	Cordon Los Nadis
CLN05	47.50379	72.95094	290	6.08	0.07	5.03	7.87	1.05	1.79	Cordon Los Nadis
CLN04	47.50712	72.95153	444	4.90	0.04	4.43	5.36	0.47	0.46	Cordon Los Nadis
CLN03	47.50985	72.95151	615	4.43	0.03	4.12	5.69	0.31	1.26	Cordon Los Nadis
CLN02	47.51231	72.95196	753	5.96	0.03	5.44	6.19	0.52	0.23	Cordon Los Nadis
CLN01	47.51434	72.95079	886	5.40	0.05	5.32	5.53	0.08	0.13	Cordon Los Nadis
Guillaume2013_DES17-A	-47.5635	-72.826	1245	7.22	0.73	4.1	10.7	3.12	3.48	Cordon Los Nadis
Guillaume2013_DES18-A	-47.5625	-72.8325	1019	4.70	0.32	4.30	5.10	0.40	0.40	Cordon Los Nadis
Guillaume2013_DES19-A	-47.5625	-72.8392	806	3.86	0.25	2.70	6.10	1.16	2.24	Cordon Los Nadis
Guillaume2013_DES20-A	-47.5638	-72.8462	594	6.13	0.28	5.10	7.10	1.03	0.97	Cordon Los Nadis
Guillaume2013_DES21-C	-47.5645	-72.8532	386	3.36	0.19	3.20	5.30	0.16	1.94	Cordon Los Nadis
Guillaume2013_DES22-A	-47.5711	-72.8652	147	3.59	0.14	3	6.70	0.59	3.11	Cordon Los Nadis
Thomson_THC14-HEA	-47.5925	-72.8515	20	3.8235	0.06366					
Thomson_THC14-FTA	-47.5925	-72.8515	20	7.6	1.1					